Journal of Materials Chemistry C

Accepted Manuscript

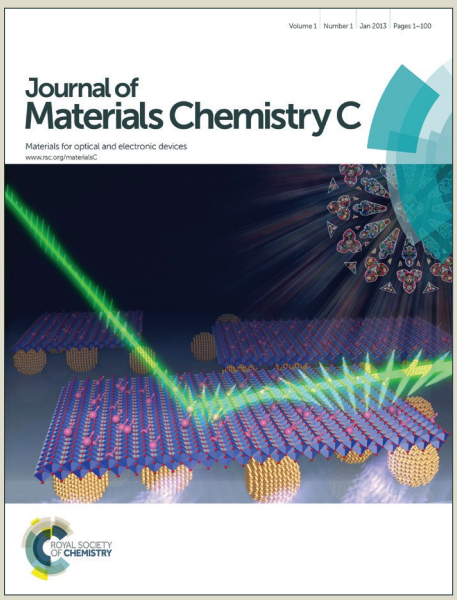

ROYAL SOCIETY OF CHEMISTRY

www.rsc.org/materialsC

Journal of Materials Chemistry C

RSCPublishing

ARTICLE

Multiscale simulation of charge transport in a host material, *N*,*N*'-dicarbazole-3,5-benzene (mCP), for organic light-emitting diodes †

Cite this: DOI: 10.1039/x0xx00000x

Received 00th January 2012,
Accepted 00th January 2012

DOI: 10.1039/x0xx00000x

www.rsc.org/

Furitsu Suzuki,[a] Katsuyuki Shizu,[a] Hisafumi Kawaguchi,[a] Shinya Furukawa,[a] Tohru Sato,[b] Kazuyoshi Tanaka,[b] and Hironori Kaji*[a]

We have performed multiscale charge transport simulations in organic amorphous thin films by explicitly considering organic molecules. The simulations were based on quantum chemical and Monte Carlo calculations. The amorphous layer was composed of *N*,*N*'-dicarbazole-3,5-benzene, which is a widely used host material in the emissive layer of blue-emitting organic light-emitting diodes. The hole mobility was calculated to be three to four times larger than the electron mobility. This trend was consistent with the experimentally obtained mobility ratio. It was also found that the charges are transported dominantly by diffusion-type character at low applied electric fields and the contribution of drift-type character increased as the applied electric field increased. The difference between the number of hops in the forward and the backward directions contributes to the actual charge transport. From the detailed molecular level analysis, it was turned out that the molecular pairs with a large electronic coupling do not necessarily have large contributions to the charge transport; rather can temporarily trap charges. We found important molecular pairs, which form effective charge-transfer paths, although the electronic coupling was not substantially large.

Introduction

Organic light-emitting diodes (OLEDs) are one of the most attractive and promising devices for application to flat/flexible ultra-thin displays and solid-state lighting sources. In 1953, the first electroluminescence (EL) from organic compounds was observed by Bernanose et al.[1] Thereafter, Helfrich et al. observed EL resulting from the recombination of holes and electrons in anthracene single crystal under an applied electric field.[2] The first multi-layered OLEDs were reported in the pioneering work of Tang and VanSlyke in 1987.[3] They have greatly improved the EL efficiency of OLEDs by the insertion of a hole transport layer between electrode and emissive/electron transport layer. Adachi et al. have further improved the EL efficiency using the multi-layered structures.[4] These early studies have emerged significant interest in OLEDs and have formed the basis of device structures of today's OLEDs.

At present, considerable efforts have been devoted to improve the luminescence efficiency.[5-10] The optimization of the charge injection and charge blocking at each interface, and charge transport in each layer is one of the crucial issues to decrease the energy loss. Among these factors, the injection and the blocking of charges have often been discussed in terms of energy levels of the highest occupied molecular orbital (HOMO) and the lowest unoccupied molecular orbital (LUMO) of organic molecules. The HOMO and the LUMO can be well estimated using quantum chemical calculations for isolated molecules. However, the charge transport in organic aggregate systems is considered to greatly depend not only on the structure of the molecule in an isolated state but also in an intermolecular aggregated state. Recently, some research groups[11-14] including our own[15, 16] have evaluated charge transport properties by quantum chemical calculations of the rate constant for charge hopping between two molecules, k_{CT}. This approach will provide some hints for the material design. However, calculated k_{CT} instead of the calculated mobility was compared against the experimental mobility in these studies. Moreover, crystal structures are used for the calculation of k_{CT} in most cases. Approaches not for crystal systems but for amorphous systems are necessary for a full understanding of OLEDs, because actual OLEDs are composed of amorphous thin layers.

We can find an approach for the understanding of charge transport properties of amorphous systems; Bässler et al.[17-19] evaluated the charge transport properties between the electrodes using Monte Carlo simulation. This is one of the most successful studies for charge transports. However, because this approach, including related studies,[20-30] does not consider the organic molecule explicitly, it is somewhat difficult to link the macroscopic charge transfer and the microscopic molecular structure directly.

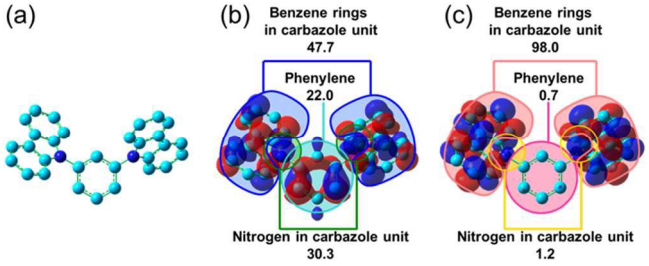

Fig. 1 (a) Molecular structure of mCP; (b) distribution of the HOMO of mCP; (c) distribution of the LUMO of mCP. The squared molecular orbital coefficients of benzene rings in carbazole unit, nitrogen in carbazole unit, and central phenylene unit are also shown in percentage.

We can assume that a detailed study of the charge transfer processes between electrodes is possible by the combination of these two approaches and such attempts have been made in recent years.[31-37] For example, Kwiatkowski et al. performed simulations of the charge mobility for an amorphous tris(8-hydroxyquinoline) aluminum (III) (Alq_3) system by approximating the Alq_3 molecule as a rigid body.[31] This is the first attempt for the charge transfer simulation considering organic molecules explicitly, as far as we know. Although the absolute value of the experimental charge mobility of Alq_3 could not be reproduced, they succeeded in explaining the difference between hole and electron mobility. They considered that this difference originated from the delocalization of the HOMO and the LUMO on the Alq_3 molecule. Lukyanov et al. constructed an Alq_3 aggregated structure using molecular dynamics (MD) simulations without applying the rigid body approximation and investigated the influence of the force fields on the charge mobility in detail.[32] However, theoretical treatment of amorphous systems is not yet well established. One of the reasons is that large-scale, high computational cost MD simulations are required to reproduce actual amorphous systems. Also, the method has been applied to Alq_3[31-36] and 2,8-bis(triphenylsilyl)-dibenzofuran (BTDF)[37], 9,10-di-(2′-naphthyl)anthracene (ADN),[38] *N*,*N*′-bis(1-naphthyl)-*N*,*N*′-diphenyl-1,1′-biphenyl-4,4′-diamine (NPD)[38] so far. The theory should be applied to other important molecular systems for the understanding of charge transfer phenomena in organic amorphous systems and for the development of excellent charge transfer materials.

In this study, we have performed multiscale charge transport simulations for the amorphous structure of *N*,*N*'-dicarbazole-3,5-benzene (mCP; shown in Fig. 1a), which has been used as a bipolar host material for the emissive layer in blue-emitting OLEDs. We also investigated the contribution of respective molecular pairs to the charge transport in amorphous thin films. We show that molecular pairs with large electronic couplings are not most important in charge transport processes. We will show some molecular pairs effectively transport charges in the forward direction, although they do not have substantially large electronic couplings. Charge transport in single crystal systems is mainly detemined by electronic coupling. However, that is not necessarily true of amorphous systems. Actual OLEDs are composed not of crystalline but of amorphous thin layers. Since the crucial factor is different in amorphous and crystal systems, the approach for amorphous systems in this study is significant for the understanding of charge transports in actual OLEDs.

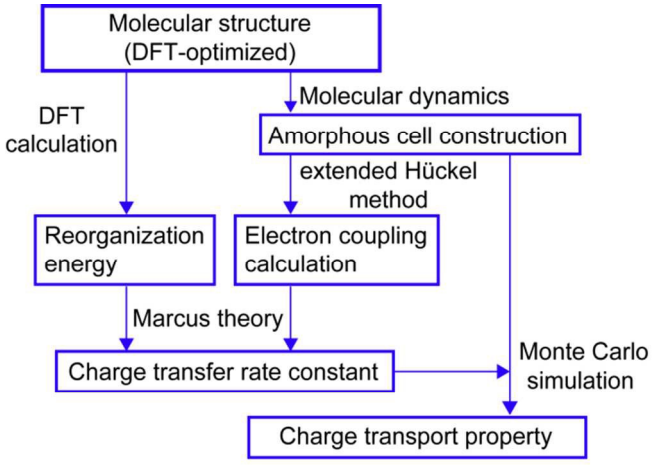

Fig. 2 Flow of the charge transport simulations for the amorphous mCP layer.

Results and discussion

The entire computational flow is shown in Fig. 2. The geometry optimization of the mCP in its neutral, cationic, and anionic states were performed using density functional theory (DFT) implemented in the Gaussian 09 program package using the B3LYP/6-31G(d) level of theory.[40] The reorganization energy for hole transport (λ^+) was obtained from the energies of the optimized structures of the neutral and cationic states. The reorganization energy for electron transport (λ^-) was calculated in a similar way. The details are provided elsewhere[15, 16]. The construction of the amorphous structure was carried out by MD simulation for 100 molecules of mCP in a cubic cell (denoted as "mCP-100"). To mimic the deposition process, the initial construction of the structure was performed at a density of 0.1 g cm^{-3} and at a temperature of 598 K. Pre-optimization was then conducted. The MD simulation was performed until the density of the system becomes constant, which was over 300 ps with the constant-pressure, constant-temperature (NPT) ensembles at 298 K. A system consists of ten molecules of mCP (denoted as "mCP-10") was also constructed in the same way. The final density of the structure was 1.0 g cm^{-3} for both the mCP-100 structure and the mCP-10 structure. The amorphous structures thus obtained are shown in Fig. S1 in ESI. The calculation of the electronic coupling for hole and electron transfer (H_{AB}^+ and H_{AB}^-, respectively) was performed for the molecular pairs that have a center-to-center distance within 20 Å in the amorphous structure. Using the values of H_{AB}^+ and λ^+ or H_{AB}^- and λ^- obtained above, the rate constants for hole and electron transfer (k_{CT}^+ and k_{CT}^-, respectively) under the applied external electric field was calculated according Eq. 1,[17, 41]

$$k_{CT}^{+/-} = \frac{4\pi^2}{h} H_{AB}^{+/-2} \frac{1}{\sqrt{4\pi\lambda^{+/-}k_B T}} \exp\left[\left(-\frac{(\lambda^{+/-}+\Delta G)^2}{4\lambda^{+/-}k_B T}\right)\right], \quad (1)$$

where ΔG is the free energy difference between the initial and final states, T is the temperature, h is Plank's constant and k_B is Boltzmann's constant. At present, Marcus theory is widely used and no crucial problems are found for treating the charge transport of organic molecules.[42-44] Under the applied external electric field, the free energy change, ΔG, is given by Eq. 2,

$$\Delta G = qF\Delta x, \quad (2)$$

where q is the elementary charge (unit charge), F is the applied external electric field strength, and Δx is the distance between the neighboring relevant molecules along the electric field. The

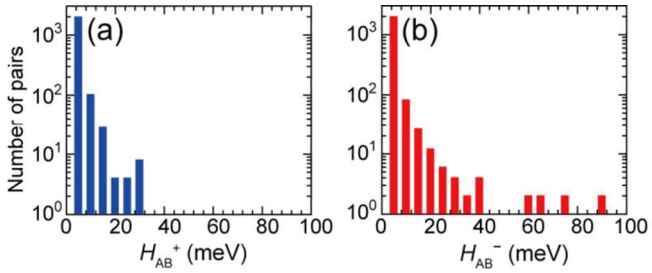

Fig. 3 Histograms of the number of pairs with the electronic coupling for (a) holes (H_{AB}^{+}) and (b) electrons (H_{AB}^{-}) in the mCP-100 structure where ΔG = 0.

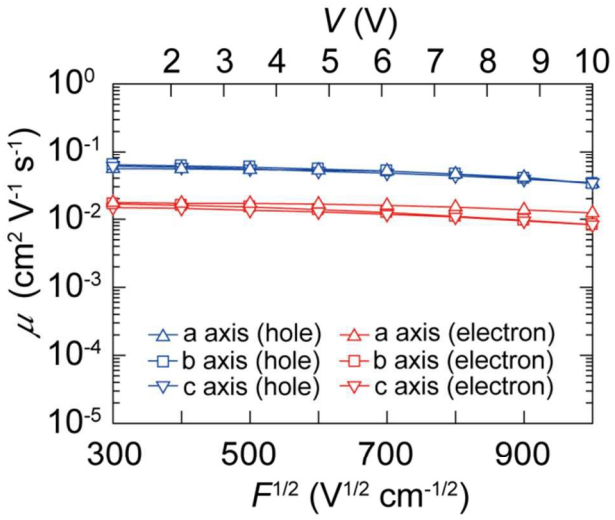

Fig. 4 Simulated field dependence of the charge mobilities for the mCP-100 structure. The thickness was set to 100 nm.

calculations of k_{CT} were performed for the pairs of molecules with a center-to-center distance within 20 Å as described above.

The charge hopping was performed using a Monte Carlo simulation based on the hopping probability corresponding to the calculated value of k_{CT}. The hoppings of 1,000 charges were simulated and the charge mobilities for holes and electrons (μ_{CT}^{+} and μ_{CT}^{-}, respectively) were calculated. The amorphous structures constructed in this study should be isotropic; therefore, the a-, b- and c-axis should be statistically equivalent. To verify this, charge transport simulations were performed by applying the electric field along the a-, b- or c-axis of the cubic cell individually. Anisotropy was observed in the charge mobility for the mCP-10 structure (Fig. S2 in ESI), so the statistical average in mCP-10 was not sufficient. As described below, the charge mobility was isotropic for the mCP-100 structure, reflecting the random distribution of mCP molecules, so the results of the calculations using the mCP-100 structure are mainly described in this paper. The reorganization energy for hole and electron transport (denoted as λ^{+} and λ^{-}, respectively) were 0.077 eV and 0.14 eV, respectively. Figure 1b and c show distribution of the HOMO and the LUMO of mCP, respectively. The squared molecular orbital coefficients of respective fragments of mCP are also shown in percentage. While the HOMO is delocalized over the entire molecule including the central phenylene moiety, the LUMO is strongly localized on the outer benzene rings in carbazole moieties. Figure 3 shows the calculated electronic coupling for hole and electron transfer (H_{AB}^{+} and H_{AB}^{-}, respectively) between the neighboring molecules in the structure of mCP-100 for $\Delta G = 0$.

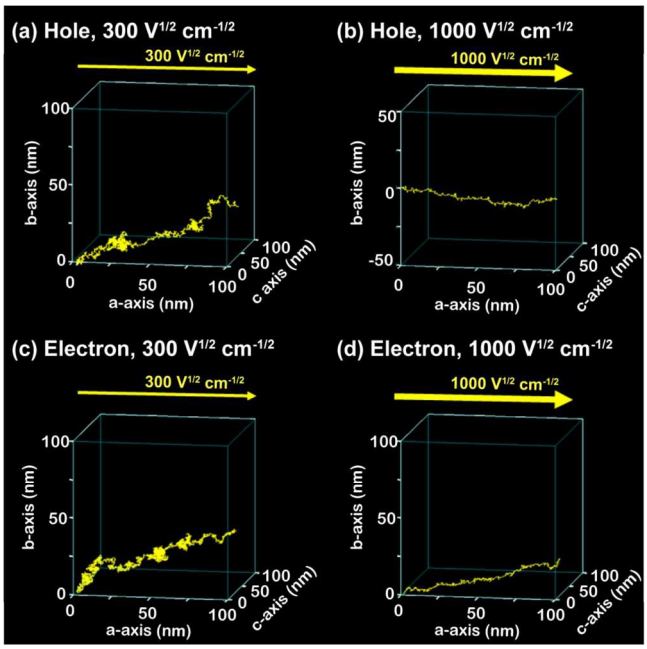

Fig. 5 Charge transfer trajectory under the electric fields applied in the direction of the a-axis: (a) hole at 300 V$^{1/2}$ cm$^{-1/2}$; (b) hole at 1000 V$^{1/2}$ cm$^{-1/2}$; (c) electron at 300 V$^{1/2}$ cm$^{-1/2}$; (d) electron at 1000 V$^{1/2}$ cm$^{-1/2}$. The simulations were started from the origin of the cell with one hole or one electron, respectively.

Compared with the values of H_{AB}^{+} (Fig. 3a), those of H_{AB}^{-} (Fig. 3b) have a larger distribution. This implies that the overlap of the LUMOs among neighboring mCP molecules is significantly increased when there is close contact of the carbazole moieties. As shown in Fig. S3a and b in ESI, the pair of molecules with the maximum value of H_{AB}^{-} ($H_{AB}^{-}{}_{max}$) has closer contact of the carbazole moieties than that with maximum value of H_{AB}^{+} ($H_{AB}^{+}{}_{max}$).

Figure 4 shows the electric field dependence of the hole and electron mobilities along the a-, b- and c-axes of the amorphous mCP-100 structure by Monte Carlo simulations. Compared with the results for the mCP-10 (see Fig. S2 in ESI), the difference in the charge mobility for the mCP-100 structure along each axis is significantly small. The mCP-100 structure can sufficiently reproduce the isotropic nature of an amorphous system. The ratio of the charge mobility for hole/electron transfer, μ^{+}/μ^{-}, varied between 2.7 and 4.2 within the range of 300–1,000 V$^{1/2}$ cm$^{-1/2}$. This suggests that the mCP-100 structure has better hole transport than electron transport. The ratio of μ^{+}/μ^{-} is almost the same as that experimentally obtained. The absolute mobilities are 1–2 orders of magnitude higher than the experimental values. [45-47] This is probably because outer-sphere reorganization energies and/or distributions of HOMO/LUMO energy levels (diagonal disorder) are ignored in our calculation. In addition, the absence of these effects would lead to the calculated negative field dependence (Fig. 4), which are inconsistent with the experimental observations. The calculation of reorganization energies can be improved, for example, by taking into account effects of surrounding molecules with a quantum mechanical/molecular mechanical method.[48] The origin of the inconsistency between calculations and experiments is now under investigation.

Figure 5 shows the charge transport trajectories for the one-hole and the one-electron simulations using the mCP-100

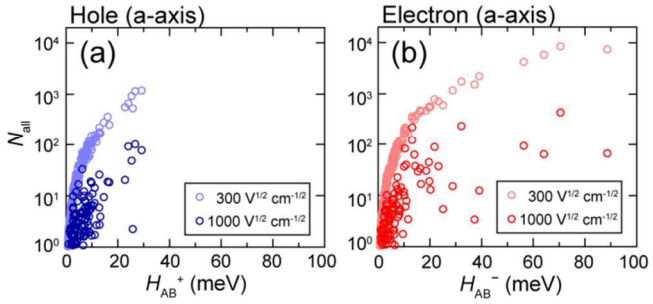

Fig. 6 Correlation of the total number of hops (N_{all}) and the electronic coupling ((a) for holes, H_{AB}^{+}, and (b) for electrons, H_{AB}^{-}) under the different electric fields in the direction of the a-axis.

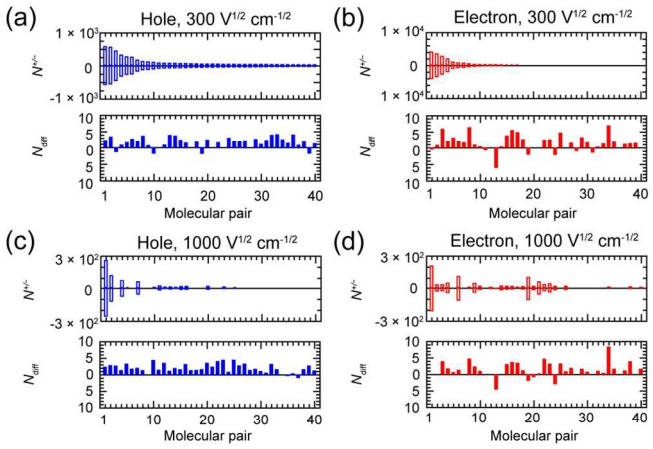

Fig. 7 Number of hops in the forward direction (N^{+}), backward direction (N^{-}), and difference (N_{diff}): (a) hole at 300 V$^{1/2}$ cm$^{-1/2}$; (b) hole at 1000 V$^{1/2}$ cm$^{-1/2}$, (c) electron at 300 V$^{1/2}$ cm$^{-1/2}$; (d) electron at 1000 V$^{1/2}$ cm$^{-1/2}$. The molecular pairs are numbered in order of decreasing N_{all} at 300 V$^{1/2}$ cm$^{-1/2}$. The top 40 molecular pairs with high N_{all} are shown in the figure. The charge transport simulations were performed with the electric field in the direction of the a-axis. The values of N^{+} and N^{-} are the averages of the 1000 times of the Monte Carlo simulations. Note that N^{+} and N^{-} are shown in positive and negative values, respectively.

structure. At 300 V$^{1/2}$ cm$^{-1/2}$, the hole (Fig. 5a) reached the counter electrode by using complicated routes, going back and forth, indicating a strong diffusive behavior. At 1,000 V$^{1/2}$ cm$^{-1/2}$, the hopping of the hole in the direction of the applied field was more efficient (Fig. 5b). The trajectories for electron transport had a similar trend depending on the applied electric field (Fig. 5c and d). These results clearly indicate that there is increased contribution of the drift transport as the applied electric field strength was increased.

As shown in Fig. 3, $H_{AB}^{-}{}_{max}$ is greater than $H_{AB}^{+}{}_{max}$. For the two molecular pairs which have $H_{AB}^{-}{}_{max}$ and $H_{AB}^{+}{}_{max}$, k_{CT}^{+} and k_{CT}^{-} were calculated according to Eqs. 1 and 2. They are denoted as $k_{CT}^{-}{}_{max}$ and $k_{CT}^{+}{}_{max}$, respectively. For 300–1,000 V$^{1/2}$ cm$^{-1/2}$, the $k_{CT}^{-}{}_{max}$ and $k_{CT}^{+}{}_{max}$ were calculated to be 9.1×10^{13} – 3.2×10^{14} s^{-1} and 2.6×10^{13} – 5.1×10^{13} s^{-1}, respectively. From the results, we expect mCP has superior electron transport property rather than hole transport. However, Monte Carlo simulations tell us that μ^{+} is larger than μ^{-} as shown in Fig. 4. To clarify the details, we analyzed the relationship of H_{AB} and the charge transport between the electrodes. Figure 6 shows the relationship of H_{AB} and the total number of hops, N_{all}. Here, N_{all} is the number of times that hopping occurred between the two molecules during the simulation (the sum of the hops in the

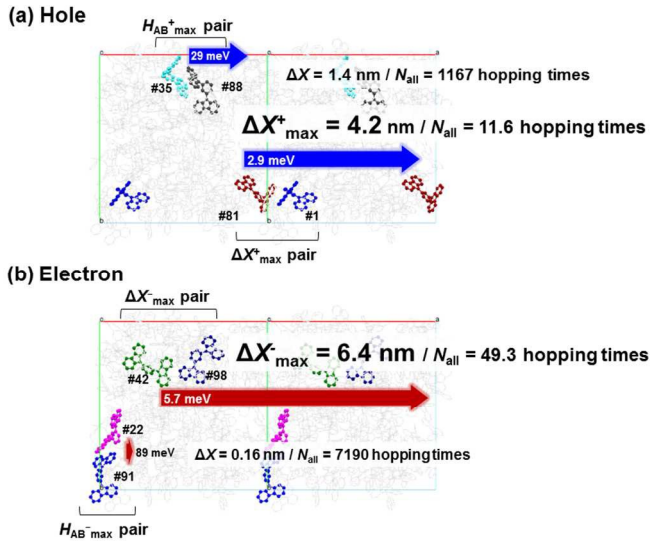

Fig. 8 The values of H_{AB}^{+}, H_{AB}^{-}, ΔX^{+}, and ΔX^{-} for the molecular pairs with $H_{AB}^{+}{}_{max}$, $H_{AB}^{-}{}_{max}$, $\Delta X^{+}{}_{max}$, and $\Delta X^{-}{}_{max}$: (a) for hole transfers and (b) electron transfers along the a-axis at a 300 V$^{1/2}$ cm$^{-1/2}$. The length of the arrow is proportional to the actual migration distance, ΔX.

forward direction (N^{+}) and in the backward direction (N^{-}); N_{all} = N^{+} + N^{-}). The values of N_{all}, N^{+}, and N^{-} are the averages of the 1000 times trials of the Monte Carlo simulations. At 300 V$^{1/2}$ cm$^{-1/2}$, N_{all} for both of holes and electrons monotonously increased with H_{AB}^{+} and H_{AB}^{-}. However, at 1,000 V$^{1/2}$ cm$^{-1/2}$, a deviation from the trend was observed. In Fig. 7a and b, N^{+}, N^{-}, and their difference (N_{diff}; $N_{diff} = N^{+} - N^{-}$) are shown for the top 40 pairs of large N_{all} at 300 V$^{1/2}$ cm$^{-1/2}$. The corresponding data for 1,000 V$^{1/2}$ cm$^{-1/2}$ is shown in Fig. 7c and d. A clear relationship was not seen between N^{+} and N_{diff}. This suggests that hopping transport may not always proceed efficiently in the forward direction even if N^{+} is high. "Round-trips", that is, carriers hop forward but return back to the original molecule, occur. As shown in Fig. 7, even though the number of hops in the forward direction, N^{+}, was greater than 10^{2}, there was approximately the same number of hops in the backward direction, N^{-}. The actual number of hops in the forward direction (N_{diff}) was at most approximately 5.

Here, we define ΔX by the product of N_{diff} and Δx:

$$\Delta X = N_{diff}\Delta x. \quad (3)$$

ΔX is the contribution of each pair for the migration distance of a charge (average migration distance of 1,000 charges) in the direction of the applied electric field. Although, no relationships were observed between H_{AB} and ΔX (Fig. S4 in ESI), and between N^{+} and ΔX (Fig. S5 in ESI), we found a correlation between N_{diff} and ΔX (Fig. S6 in ESI). These results show that the charge transport is not uniquely determined by the value of H_{AB} in the case of amorphous systems. This is different from the crystal systems.[15, 16]

Figure 8 shows the pairs with $H_{AB}^{+}{}_{max}$, $H_{AB}^{-}{}_{max}$, the pairs with the largest migration distance, $\Delta X^{+}{}_{max}$ and $\Delta X^{-}{}_{max}$, in the amorphous structure, respectively (see also Fig. S3 in ESI). While $\Delta X^{+}{}_{max}$ is 4.2 nm for hole transport (the H_{AB}^{+} is 2.9 meV), ΔX^{+} of the pair with $H_{AB}^{+}{}_{max}$ (29 meV) is only 1.4 nm. For electron transport, $\Delta X^{-}{}_{max}$ is 6.4 nm (the H_{AB}^{-} is 5.7 meV), whereas ΔX^{-} is only 0.16 nm for the molecular pair with $H_{AB}^{-}{}_{max}$ (89 meV). Table 1 summarizes N^{+}, N^{-}, N_{all}, and N_{diff} for the respective molecular pairs shown in Fig. 7. The ratio, N_{all} / N_{diff}, and ΔX are also shown. For the molecular pairs with $H_{AB}^{+}{}_{max}$, the charges hopped in the direction of the applied

Table 1 Number of hops in the forward direction (N^+), backward direction (N^-), the sum (N_{all}), and the difference (N_{diff}) for the respective molecular pairs shown in Fig. 8. The ratio of N_{all} / N_{diff} and the average migrated distance (ΔX) are also shown.

Molecule Pairs	$H_{AB}^{+/-}$ (meV)	$F^{1/2}$ ($V^{1/2}$ $cm^{-1/2}$)	Number of hops				N_{all} /N_{diff}	ΔX (nm)
			N^+	N^-	N_{all}	N_{diff}		
$H_{AB}^{+}{}_{max}$	29	300	584.7	582.4	1167.1	2.3	515	1.4
		1000	40.2	35.9	76.1	4.3	18	2.7
$\Delta X^{+}{}_{max}$	2.9	300	8.0	3.6	11.6	4.4	3	4.2
		1000	5.8	0.0	5.8	5.8	1	5.5
$H_{AB}^{-}{}_{max}$	89	300	3595.3	3594.5	7189.8	0.8	9289	0.16
		1000	32.2	32.1	64.3	0.1	495	0.026
$\Delta X^{-}{}_{max}$	5.7	300	27.2	22.1	49.3	5.1	10	6.4
		1000	7.8	0.2	8.0	7.6	1	9.6

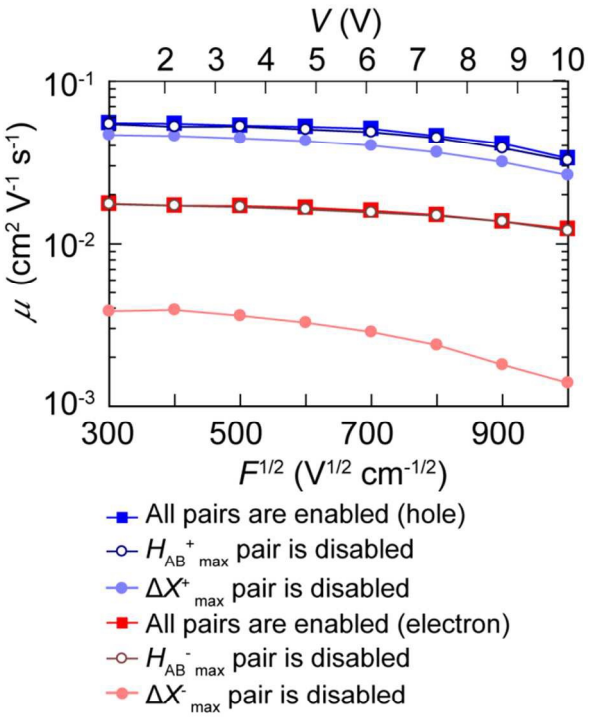

Fig. 9 Simulation of the charge mobility with the molecular pairs with $H_{AB}^{+}{}_{max}$, $H_{AB}^{-}{}_{max}$, $\Delta X^{+}{}_{max}$ and $\Delta X^{-}{}_{max}$ either enabled or disabled. The thickness of the charge transport layer was set to 100 nm.

electric field once in every 515 times of hops at 300 $V^{1/2}$ $cm^{-1/2}$, and it became approximately once in every 18 times of hops at 1,000 $V^{1/2}$ $cm^{-1/2}$. It is clear that while the diffusion transport is dominant at low applied electric fields, the contribution of the drift transport increased as the applied electric field increased. For the molecular pairs with $\Delta X^{+}{}_{max}$, the charges hop in the direction of the applied field once in every 3 times of hops at 300 $V^{1/2}$ $cm^{-1/2}$. The charges hopped almost every time in the direction of the applied electric field when the field was increased to 1000 $V^{1/2}$ $cm^{-1/2}$. The hops for the molecular pairs with $\Delta X^{-}{}_{max}$ and $H_{AB}^{-}{}_{max}$ showed similar trends to those with $\Delta X^{+}{}_{max}$ and $H_{AB}^{+}{}_{max}$. Charge-hopping for the molecular pairs with $H_{AB}^{+}{}_{max}$ and $H_{AB}^{-}{}_{max}$ occurred mainly through diffusion, resulting that charges tend to take "round-trips" between the two molecules, especially at low electric fields. For molecular pairs with $\Delta X^{+}{}_{max}$ and $\Delta X^{-}{}_{max}$, the contribution of the drift transport increased. For the pairs with large ΔX, the free energy difference between the initial and final states, ΔG, is large as found from Eqs. 2 and 3. The large ΔG is the origin of the effective forward hopping.

Figure 9 shows the results of the charge transport simulations (the electric field is applied along the a-axis). The hole and electron mobilities along the a-axis in Fig. 5 are replotted in Fig. 9 as filled squares. Compared to these, both hole and electron mobilities were reduced when the molecular pairs with $\Delta X^{+}{}_{max}$ or $\Delta X^{-}{}_{max}$ was not used for charge transport simulations (filled circles). In particular, the electron mobility reduced significantly. It is obvious that the molecular pairs with $\Delta X^{+}{}_{max}$ and $\Delta X^{-}{}_{max}$ form a critical hopping path for charge transports and improve charge mobilities. In sharp contrast, both hole and electron mobilities were unchanged, regardless of whether the molecular pair with $H_{AB}^{+}{}_{max}$ (or $H_{AB}^{-}{}_{max}$) were used (filled squares) or not (open circles). These results show that the molecular pairs with $H_{AB}^{+}{}_{max}$ and $H_{AB}^{-}{}_{max}$ are not critical for charge transports between electrodes. The electron mobility of mCP would be increased by increasing ΔX and decreasing its distribution. Such distribution can be realized when molecular pairs with moderately large H_{AB}^{-} and intramolecular distance (Δx) are placed regularly.

Conclusions

In this study, we performed the charge transport simulations in an amorphous mCP thin layer. Organic molecules were explicitly considered to link the macroscopic charge transfer and the microscopic molecular structure directly. The hole mobility of mCP was calculated to be three to four times larger than the electron mobility. This result was in good agreement with the experimentally determined ratio of the charge mobility for hole and electron transfer. It was clearly shown that while the diffusion transport is dominant at low applied electric fields, the contribution of the drift transport increased as the applied electric field increased. At a low electric field strength, both holes and electrons reached the counter electrode not through simple routes directly toward the direction of the applied electric field but through complicated routes, including the direction opposite to and perpendicular to the electric field. At a high electric field strength, charge hopping in the direction of the applied electric field can be advantageous and becomes significantly efficient. Charge hopping for molecular pairs with large H_{AB} was mainly diffusive and back and forth between the two molecules tended to occur more frequently. Therefore, these molecular pairs are not crucial for charge transports. In contrast, the contribution of the drift transport was dominant for molecular pairs with large ΔX. The molecular pair substantially improve charge mobilities by forming effective charge transfer path.

We revealed that one of the important factor of charge transport in amorphous systems is relative configuration of the molecules rather than H_{AB}. This is different from the charge transport in crystal systems. Our findings are important not only

for fundamental science but also for the design of charge-transporting materials by controlling electronic states and intermolecular orientation. Further development of this approach is in progress for multi-layered amorphous systems composed of hole transport, emission, and electron transport layers, and for more complex systems, including charge blocking layers, etc.

Computational methods

The Dreiding force field was used for the MD simulation. The MD simulations were carried out under periodic boundary conditions. The parameters for the Dreiding force field such that the MD simulation reproduced the molecular structure of mCP optimized with DFT method (for more details, see Fig. S7 in ESI and Tables S1, S2). The total number of pairs, approximately 270,000, was reduced to about 5,000 pairs at the 20 Å cut-off for the calculation of H_{AB}^{+} and H_{AB}^{-}. As shown in Fig. S8 in ESI, the values of H_{AB} of the molecular pairs, whose adjacent center-to-center distance is more than 20 Å, is negligibly small, less than 1×10^{-10} meV. We verified that these molecular pairs with small H_{AB} do not take part in the charge transport. For Monte Carlo simulations, periodic boundary conditions were set in all directions. The thickness of the film was 100 nm and the electric field was applied in this direction for the charge transport simulation. The square root of the external electric field was 300–1,000 $V^{1/2}$ $cm^{-1/2}$, which corresponded to a voltage of 0.9–10 V. The temperature was set to 298 K. Amorphous cell and Forcite programs (Accelrys Inc., San Diego, CA, USA) were used for the construction of the amorphous structure. Calculations of H_{AB} was performed by the Gaussian 09 program package using the extended Hückel theory and in-house program written in C. Charge transport Monte Carlo simulations was performed using the in-house C program.

Acknowledgements

This research was funded by the JSPS FIRST Program initiated by CSTP and KAKENHI. The calculations were supported by supercomputer system at ICR, Kyoto University.

Notes and references

[a]*Institute for Chemical Research, Kyoto University, Uji, Kyoto 611-0011, Japan. E-mail: kaji@scl.kyoto-u.ac.jp*
[b]*Department of Molecular Engineering, Graduate School of Engineering, Kyoto University, Kyoto 615-8510, Japan.*
† Electronic Supplementary Information (ESI) available. See DOI: 10.1039/b000000x/

1. A. Bernanose, *J. Chim. Phys*, 1953, **50**, 64.
2. W. Helfrich and W. G. Schneider, *Phys. Rev. Lett.*, 1965, **14**, 229.
3. C. W. Tang and S. A. VanSlyke, *Appl. Phys. Lett.*, 1987, **51**, 913.
4. C. Adachi, T. Tsutsui and S. Saito, *Appl. Phys. Lett.*, 1989, **55**, 1489.
5. C. Hosokawa, H. Higashi, H. Nakamura and T. Kusumoto, *Appl. Phys. Lett.*, 1995, **67**, 3853.
6. J. Kido, M. Kimura and K. Nagai, *Science*, 1995, **267**, 1332.
7. R. Abbel, C. Grenier, M. J. Pouderoijen, J. W. Stouwdam, P. E. L. G. Leclère, R. P. Sijbesma, E. W. Meijer and A. P. H. J. Schenning, *J. Am. Chem. Soc.*, 2008, **131**, 833.
8. A. C. Grimsdale, K. Leok Chan, R. E. Martin, P. G. Jokisz and A. B. Holmes, *Chem. Rev.*, 2009, **109**, 897.
9. C. Yuan, S. Saito, C. Camacho, S. Irle, I. Hisaki and S. Yamaguchi, *J. Am. Chem. Soc.*, 2013, **135**, 8842.
10. S. Reineke, M. Thomschke, B. Lüssem and K. Leo, *Rev. Mod. Phys.*, 2013, **85**, 1245.
11. B. C. Lin, C. P. Cheng, Z. Q. You and C. P. Hsu, *J. Am. Chem. Soc.*, 2005, **127**, 66.
12. C. Lee and K. Sohlberg, *Chem. Phys.*, 2010, **367**, 7.
13. H. Gao, *Theor. Chem. Acc.*, 2010, **127**, 759.
14. B. C. Lin, C. P. Cheng, Z. Q. You and C. P. Hsu, *Phys. Chem. Chem. Phys.*, 2011, **13**, 20704.
15. T. Yamada, T. Sato, K. Tanaka and H. Kaji, *Org. Electron.*, 2010, **11**, 255.
16. T. Yamada, F. Suzuki, A. Goto, T. Sato, K. Tanaka and H. Kaji, *Org. Electron.*, 2011, **12**, 169.
17. H. Bässler, *Phys. Status Solidi B*, 1993, **175**, 15.
18. H. Bässler and B. Schweitzer, *Acc. Chem. Res.*, 1999, **32**, 173.
19. I. I. Fishchuk, A. Kadashchuk, H. Bässler and S. Nešpůrek, *Phys. Rev. B*, 2003, **67**, 2243031.
20. D. H. Dunlap, P. E. Parris and V. M. Kenkre, *Phys. Rev. Lett.*, 1996, **77**, 542.
21. A. Hirao and H. Nishizawa, *Phys. Rev. B*, 1996, **54**, 4755.
22. A. Hirao and H. Nishizawa, *Phys. Rev. B*, 1997, **56**, R2904.
23. S. V. Novikov, D. H. Dunlap, V. M. Kenkre, P. E. Parris and A. V. Vannikov, *Phys. Rev. Lett.*, 1998, **81**, 4472.
24. A. Ohno and J. Hanna, *Appl. Phys. Lett.*, 2003, **82**, 751.
25. S. Yin and Y. Lv, *Org. Electron.*, 2008, **9**, 852.
26. J. J. M. Van Der Holst, F. W. A. Van Oost, R. Coehoorn and P. A. Bobbert, *Phys. Rev. B*, 2011, **83**, 085206.
27. A. Troisi, *Chem. Soc. Rev.*, 2011, **40**, 2347.
28. S. Ciuchi and S. Fratini, *Phys. Rev. B*, 2012, **86**, 245201.
29. S. R. Mohan, M. P. Singh, M. P. Joshi and L. M. Kukreja, *J. Phys. Chem. C*, 2013, **117**, 24663.
30. V. R. Nikitenko and M. N. Strikhanov, *J. Appl. Phys.*, 2014, **115**, 073704.
31. J. J. Kwiatkowski, J. Nelson, H. Li, J. L. Bredas, W. Wenzel and C. Lennartz, *Phys. Chem. Chem. Phys.*, 2008, **10**, 1852.
32. A. Lukyanov, C. Lennartz and D. Andrienko, *Phys. Status Solidi A:*, 2009, **206**, 2737.
33. J. Nelson, J. J. Kwiatkowski, J. Kirkpatrick and J. M. Frost, *Acc. Chem. Res.*, 2009, **42**, 1768.
34. B. Baumeier, F. May, C. Lennartz and D. Andrienko, *J. Mater. Chem.*, 2012, **22**, 10971.
35. A. Fuchs, T. Steinbrecher, M. S. Mommer, Y. Nagata, M. Elstner and C. Lennartz, *Phys. Chem. Chem. Phys.*, 2012, **14**, 4259.
36. V. Rühle, A. Lukyanov, F. May, M. Schrader, T. Vehoff, J. Kirkpatrick, B. Baumeier and D. Andrienko, *J. Chem. Theory Comput.*, 2011, **7**, 3335.
37. F. May, M. Al-Helwi, B. Baumeier, W. Kowalsky, E. Fuchs, C. Lennartz and D. Andrienko, *J. Am. Chem. Soc.*, 2012, **134**, 13818.
38. H. Li, L. Duan, Y. Sun, D. Zhang, L. Wang, Y. Qiu, *J. Phys. Chem. C*, 2013, **117**, 16336.
39. P. Friederich, F. Symalla, V. Meded, T. Neumann, W. Wenzel, *J. Chem. Theory. Comput.* 2014, **10**, 3720.
40. M. J. Frisch, G. W. Trucks, H. B. Schlegel, G. E. Scuseria, M. A. Robb, J. R. Cheeseman, G. Scalmani, V. Barone, B. Mennucci, G. A. Petersson, H. Nakatsuji, M. Caricato, X. Li, H. P. Hratchian, A. F.

Izmaylov, J. Bloino, G. Zheng, J. L. Sonnenberg, M. Hada, M. Ehara, K. Toyota, R. Fukuda, J. Hasegawa, M. Ishida, T. Nakajima, Y. Honda, O. Kitao, H. Nakai, T. Vreven, J. A. Montgomery, J. E. Peralta, F. Ogliaro, M. Bearpark, J. J. Heyd, E. Brothers, K. N. Kudin, V. N. Staroverov, R. Kobayashi, J. Normand, K. Raghavachari, A. Rendell, J. C. Burant, S. S. Iyengar, J. Tomasi, M. Cossi, N. Rega, J. M. Millam, M. Klene, J. E. Knox, J. B. Cross, V. Bakken, C. Adamo, J. Jaramillo, R. Gomperts, R. E. Stratmann, O. Yazyev, A. J. Austin, R. Cammi, C. Pomelli, J. W. Ochterski, R. L. Martin, K. Morokuma, V. G. Zakrzewski, G. A. Voth, P. Salvador, J. J. Dannenberg, S. Dapprich, A. D. Daniels, Ö. Farkas, J. B. Foresman, J. V. Ortiz, J. Cioslowski and D. J. Fox, Gaussian 09, Gaussian Inc. Wallingford, CT, 2009.

41. R. A. Marcus and N. Sutin, *Biochim. Biophys. Acta*, 1985, **811**, 265.
42. C. Poelking, E. Cho, A. Malafeev, V. Ivanov, K. Kremer, C. Risko, J. L. Brédas and D. Andrienko, *J. Phys. Chem. C*, 2013, **117**, 1633.
43. N. R. Tummala, S. Mehraeen, Y. T. Fu, C. Risko and J. L. Brédas, *Adv. Funct. Mater.*, 2013, **23**, 5800.
44. S. R. Yost, J. Lee, M. W. B. Wilson, T. Wu, D. P. McMahon, R. R. Parkhurst, N. J. Thompson, D. N. Congreve, A. Rao, K. Johnson, M. Y. Sfeir, M. G. Bawendi, T. M. Swager, R. H. Friend, M. A. Baldo and T. Van Voorhis, *Nat. Chem.*, 2014, **6**, 492.
45. M. F. Wu, S. J. Yeh, C. T. Chen, H. Murayama, T. Tsuboi, W. S. Li, I. Chao, S. W. Liu and J. K. Wang, *Adv. Funct. Mater.*, 2007, **17**, 1887.
46. C. H. Hsiao, S. W. Liu, C. T. Chen and J. H. Lee, *Org. Electron.*, 2010, **11**, 1500.
47. T. Tsuboi, *J. Non-Cryst. Solids*, 2010, **356**, 1919.
48. H. Li, L. Duan, D. Zhang, Y. Qiu, *J. Phys. Chem. C*, 2014, **118**, 14848.

Journal of Materials Chemistry C

RSCPublishing

ARTICLE

Table of contents entry

By considering organic molecules explicitly, we could successfully link the macroscopic charge transfer and the microscopic molecular structure directly.